THE JOURNAL OF PHYSICAL CHEMISTRY Letters

Letter

Cite This: J. Phys. Chem. Lett. 2019, 10, 2487−2492

pubs.acs.org/JPCL

Water Ordering on the Magnetite Fe_3O_4 Surfaces

Eman Zaki,[†] Zdenek Jakub,[‡] Francesca Mirabella,[†,‡] Gareth S. Parkinson,[‡] Shamil Shaikhutdinov,*[,†] and Hans-Joachim Freund[†]

[†]Abteilung Chemische Physik, Fritz-Haber-Institut der Max-Planck-Gesellschaft, Faradayweg 4-6, 14195 Berlin, Germany

[‡]Institut für Angewandte Physik, TU Wien, Wiedner Hauptstr. 8-10, 1040 Vienna, Austria

Supporting Information

ABSTRACT: The interaction of water with the most prominent surfaces of Fe_3O_4, (001) and (111), is directly compared using a combination of temperature-programmed desorption, temperature-programmed low energy electron diffraction (TP LEED), and scanning probe microscopies. Adsorption on the $(\sqrt{2} \times \sqrt{2})R45°$-reconstructed surface of $Fe_3O_4(001)$ is strongly influenced by the surface reconstruction, which remains intact at all coverages. Close to the completion of the first monolayer, however, the ad-layer adopts a longer-range (2×2) superstructure. This finding is discussed in the context of a similar (2×2) superstructure recently observed on the (111) facet, which exists over a significantly larger range of temperatures and coverages. In both cases, the long-range order is evidence that water−water interactions exert a significant influence on the structure already prior to the nucleation of the second layer. We conclude that the stability differences stem from the smaller unit cell on the (111) surface, and the ability of water to more easily form stable hexagonal ice-like structures on the hexagonal substrate.

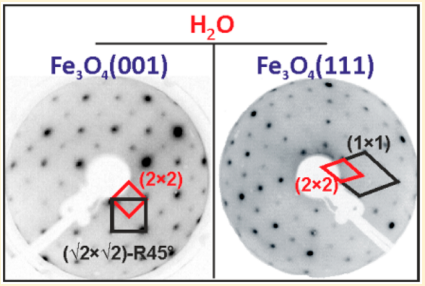

The interaction of water with oxides, in particular with iron oxides, plays an important role in geology, electrochemistry, corrosion, and catalysis.[1,2] Magnetite (Fe_3O_4) is one of the most explored oxide materials that have been studied using a "surface-science" approach.[3−5] Prepared either as single crystals or thin films, the (111) and (001) surfaces of Fe_3O_4 were investigated intensively, primarily by scanning tunneling microscopy (STM) and low energy electron diffraction (LEED), in combination with density functional theory (DFT) calculations.[4,6−12] For the (111) surface (Figure 1b), the results favor the single metal surface termination, i.e., the outmost layer consists of the tetrahedrally coordinated Fe_{tet} ions placed with a (2×2) periodicity in the 3-fold hollow sites over the close packed O-layer. (Since this is a bulk-truncation at the Fe_{tet} layer, we will refer to it as (1×1) in this Letter.) As far as the $Fe_3O_4(001)$ surface is concerned, it reconstructs upon preparation in ultrahigh vacuum (UHV) into a $(\sqrt{2} \times \sqrt{2})R45°$ structure, which was debated in the literature for a while.[4] To date, it is generally accepted that the surface reconstruction originates from an ordered array of subsurface iron vacancies and interstitials (Figure 1c).[9] The subsurface rearrangement distorts the surface lattice and causes two surface oxygen atoms without a subsurface Fe_{tet} neighbor (labeled with a yellow star in Figure 1c) to be significantly more reactive than the others. Adsorbates including atomic H and various metals have been found to bind strongly in this location.[4]

There are several experimental and theoretical studies of water adsorption on these two surfaces that were discussed within existing structural models (see refs 13−18 and references therein). Our recent temperature-programmed desorption (TPD), single crystal adsorption calorimetry, and infrared reflection absorption spectroscopy (IRAS) results, corroborated by DFT calculations, provided compelling evidence that water first dissociates on the $Fe_3O_4(111)$ surface, ultimately resulting in two surface hydroxyls. These then act as an anchor for another water molecule, resulting in a half-dissociated complex ("dimer"). At further increasing coverage, but before the formation of an amorphous solid water (ASW) film sets in, the water ad-layer forms an ordered $Fe_3O_4(111)$-(2×2) structure, as directly observed by LEED.[15,16] The observation of water ordering was, in fact, inspired by the TPD spectra showing sharp desorption peaks at relatively high coverages (Figure 2a). (NB: In these experiments, water was dosed at 140 K solely to minimize the contribution of the ASW signal in TPD spectra.) All three peaks followed first order desorption kinetics indicating the presence of water molecules having discrete binding energies and desorbing almost simultaneously at certain temperature (i.e., 200, 220, and 255 K), hence implying a certain degree of ordering. LEED movies recorded while heating the sample with the same heating rate as for TPD measurements (henceforth referred to as temperature-programmed (TP) LEED)) allowed to link water ordering and the corresponding temperature, hence water coverage. This is illustrated in Figure 2b, where the intensity of the (2×2) superstructure spots is shown as a function of temperature together with the water desorption profile. Clearly, the (2×2) structure only forms after water desorbs via the peak at 200 K. Importantly, its formation only

Received: March 18, 2019
Accepted: April 30, 2019
Published: April 30, 2019

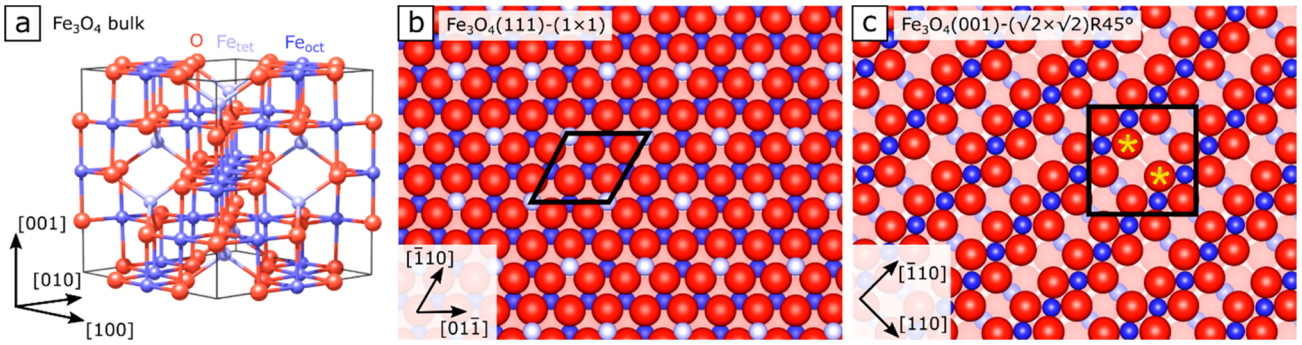

Figure 1. (a) Unit cell of Fe_3O_4 has the spinel structure. The lattice is based on a close packed oxygen lattice with octahedrally coordinated Fe (Fe_{oct}) and tetrahedrally coordinated (Fe_{tet}) cations. (b) Fe_3O_4(111) surface is terminated by Fe_{tet} cations above a close packed layer of oxygen. (c) Fe_3O_4(001) surface terminated with an intact layer of oxygen and Fe_{oct} atoms. However, a rearrangement of the subsurface cations distorts the structure leading to a $(\sqrt{2} \times \sqrt{2})$R45° superstructure. The surface oxygen atoms marked with a yellow star differ from the others as they have no subsurface Fe_{tet} neighbor.

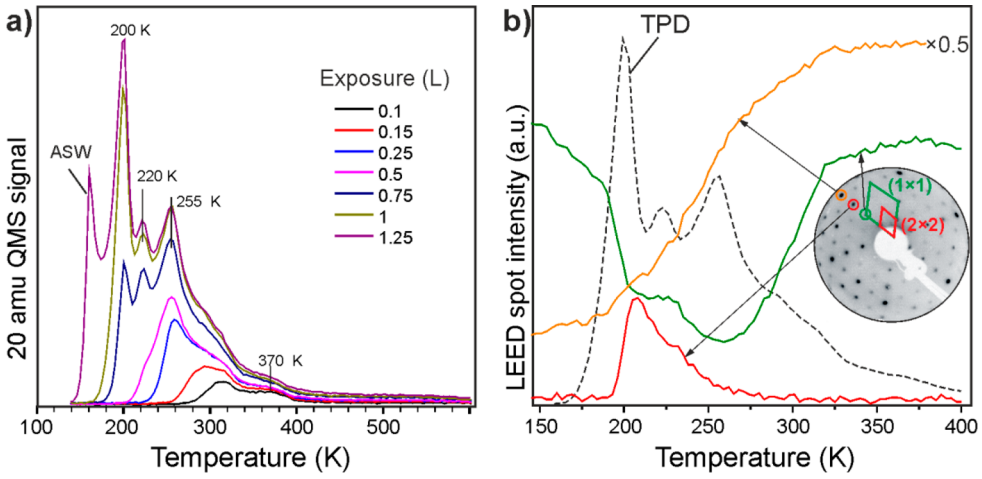

Figure 2. (a) TPD spectra of D_2O (20 amu) adsorbed on the Fe_3O_4(111) surface at 140 K at increasing exposures. The heating rate was 3 K/s. (b) Intensity of the selected diffraction spots taken from the TP LEED movie (at 64 eV) on the sample exposed to 1 L of D_2O at 140 K. The snapshot at 220 K is shown in the inset, and the unit cells are indicated. The 1 L TPD spectrum is shown as dashed line.\

depends on water coverage and not on the adsorption temperature: the (2 × 2) LEED pattern appears on samples kept at all temperatures between 200 and 250 K at water exposures resulting in coverages above some threshold, although close to saturation coverage at this temperature. Therefore, the observed long-range ordering is thermodynamically driven and not kinetically limited and only occurs at average coverages between 1.2 and 1.8 ML as determined by calibration of a mass spectrometer.[15] (Here, 1 ML is defined as one H_2O molecule per Fe_3O_4(111) unit cell exposing one Fe ion, i.e., 3.2×10^{14} at cm^{-2}.)

In addition, Figure 2b shows integral intensities of selected (0,1) and (0,1/2) spots, which mostly characterize the O- and Fe-layers in Fe_3O_4(111), respectively. In principle, the intensity of a diffraction spot depends on the incident electron energy. The so-called $I-V$ curves for several different spots are used for a quantitative analysis of ordered surface structures. In fact, it was the LEED analysis that provided compelling evidence for the currently accepted models of both the Fe_3O_4(111)[6,8] and Fe_3O_4(001)-$(\sqrt{2} \times \sqrt{2})$R45° surfaces.[9] Basically, the surface geometry determines the positions of the peaks in $I-V$ curves, whereas their intensities additionally include inelastic losses and thermal vibrations. Obviously, the adsorbate layer may alter the $I-V$ curve, both peak position and its intensity, thus leading to intensity changes at the energy monitored. Accordingly, thermal desorption results in reverse changes. Figure 2b shows that the intensity of the (0,1) spot gradually increases upon heating. This can reasonably be explained by water desorption from the surface. Meanwhile, the intensity of the (0,1/2) spot, related to the Fe sublattice and mostly to the Fe topmost layer, exhibits nonmonotonic behavior and somewhat "mirrors" the TPD curve. It rapidly decreases with the onset of the water desorption and starts to increase at temperatures above 250 K, following recombinative desorption of hydroxyl species that are only remaining at the surface at these temperatures. Clearly, the intensity drop obtained at 150−250 K is linked to the shift of the $I-V$ curve in the region close to the energy used here (64 eV), which suggests substantial changes in the Fe_{tet}−O interlayer distance at the oxide surface. This is likely due to the bond of the terminal hydroxyl to the Fe_{tet} ion. To date, acquisition of the whole $I-V$ data set during sample heating, which would shed more light on the TP LEED results, remains technically challenging.

To examine whether water adsorption on magnetite depends on the surface plane, we have carried out similar experiments on the Fe_3O_4(001) films grown on Pt(001).[12] The prepared films all showed sharp LEED patterns of the Fe_3O_4(001)-($\sqrt{2}$

DOI: 10.1021/acs.jpclett.9b00773
J. Phys. Chem. Lett. 2019, 10, 2487−2492

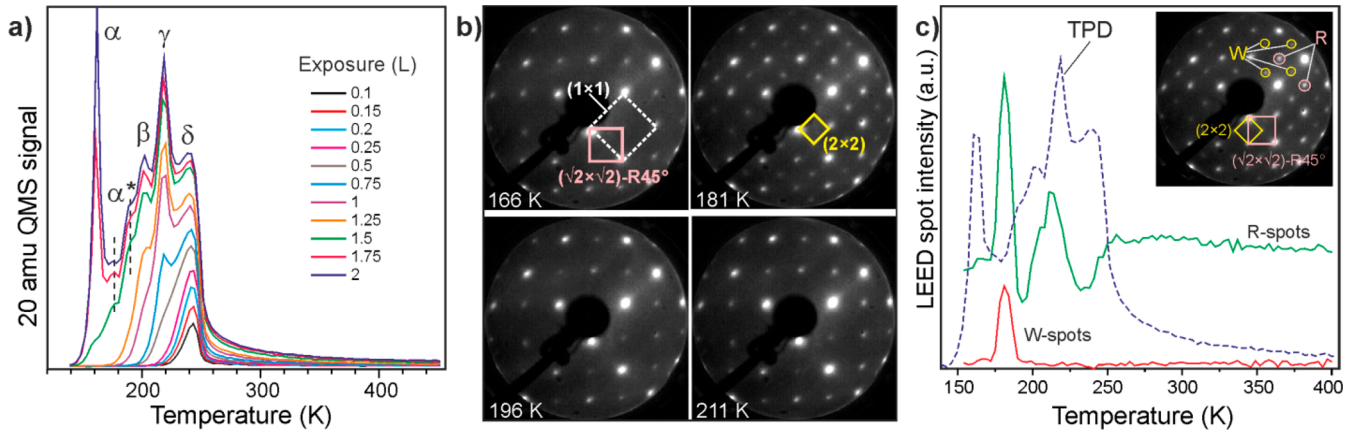

Figure 3. (a) TPD spectra of D_2O (20 amu) adsorbed on the $Fe_3O_4(001)$-$(\sqrt{2} \times \sqrt{2})R45°$ surface at 140 K. The heating rate was 3 K/s. (b) Four snapshots taken from the TP LEED movie (at 47 eV) recorded after the sample was exposed to 1.75 L of D_2O at 140 K. The unit cells are indicated. (c) Averaged intensity of the selected (circled) diffraction spots taken from the TP LEED movie (at 47 eV) on the film exposed to 1.75 L. W- and R-spots are the fingerprints of the (2 × 2) water ad-layer and $(\sqrt{2} \times \sqrt{2})R45°$ reconstructed surface, respectively. The TPD spectrum at 1.75 L exposure is shown as dashed line.

$\times \sqrt{2})R45°$ surface. Figure 3a shows TPD spectra obtained after D_2O exposure at 140 K. Three desorption states at 200, 220, and 240 K are populated with increasing exposure following first-order (or close to) desorption kinetics. The spectra look almost identical to those recently reported by some of the present authors on a $Fe_3O_4(001)$ single crystal,[17] which was additionally characterized by STM to confirm its surface termination.[9] Therefore, we may cross-correlate the results obtained in these two studies. For consistency, we label the desorption peaks α, β, etc., as in ref 17. Note that two more desorption states at around 180 K could be resolved in our experiments, which appear between the α and β peaks, henceforth denoted as α*. These were observed on many samples studied, independently of the heating rate and deposition flux. To some extent, they resemble the α' state mentioned in the previous TPD study on the single crystal surface, which was performed with a heating rate of 1 K/s.[17]

A comparison of the TPD spectra presented in Figures 2a and 3a reveals some similarities and some differences. Beyond the peak at ∼160 K, associated with a "multilayer" ASW film, three distinct desorption peaks are observed on both surfaces. Moreover, the position of the β and γ peaks on the (001) films almost coincide with desorption maxima at 200 and 220 K obtained on the (111) films, all assigned to molecular water adsorption. Substantial differences are found at higher temperatures. While the desorption from the (111) surface exhibits a maximum at 255 K and a long "tail" extending to 400 K showing a second-order desorption kinetics of dissociated species, water desorbs from the $Fe_3O_4(001)$-$(\sqrt{2} \times \sqrt{2})R45°$ surface via the 240 K peak following pseudo first-order desorption kinetics, showing a steep descending edge. This indicates that water adsorption is either nondissociative or that the hydroxyl groups resulting from dissociation do not separate on the surface during the TPD ramp and readily recombine.

As in the case of $Fe_3O_4(111)$, the sharp desorption signals observed in TPD spectra on the $Fe_3O_4(001)$ films suggest water ordering. To investigate further, we employed TP LEED, as above. Figure 3b shows four snapshots from the TP LEED movie recorded during heating the sample dosed with 1.75 L of D_2O at 140 K. Additional diffraction spots, which are identified as the $Fe_3O_4(001)$-(2 × 2) structure, were observed at 175−187 (±3) K (Figure 3c), i.e., in a much narrower temperature region as compared to the $Fe_3O_4(111)$ surface (i.e., 200−250 K, see Figure 2b). This renders its observation rather difficult and easy to overlook. Indeed, initial water coverage considerably affects the appearance of the (2 × 2) structure. At 1.5 L exposure and below, no such structure was detected, suggesting the water coverage is not sufficient to form it. The (2 × 2) structure is most markedly observed on heating of the sample exposed to 1.75 L water. At 2 L exposure, the (2 × 2) spot intensity is considerably reduced, and it further decreases at increasing exposures from 2.5 to 4, and 5 L. No LEED pattern could be observed on the 6 L sample. Comparison with the corresponding TPD spectra shows that the (2 × 2) pattern only appears after multilayer desorption and disappears before water starts to desorb via the β peak at 200 K (Figure 3c), which is in the region of the α* state. As a result, a temperature window for its observation becomes smaller at higher water coverages since the ASW desorption follows zero-order desorption kinetics, with the peak shifting toward higher temperatures. In comparison, long-range water ordering on the $Fe_3O_4(111)$ surface occurs at considerably higher temperatures (Figure 2b), and its observation is therefore less sensitive to the initial water coverage above a certain threshold.

Figure 3c also shows a temperature profile for the intensity of the diffraction spots reflecting the reconstructed surface (R-spots), which seems to be even more complex than for the (111) surface. Nevertheless, it is clear that the $(\sqrt{2} \times \sqrt{2})R45°$ surface reconstruction is maintained on the water covered surface at our conditions. For comparison, previous LEED studies have reported that the reconstruction is lifted, either upon exposure to 2×10^{-6} mbar of H_2O at 273 K for 2 min (i.e., ∼300 L) in ref 19 on a single crystal or even to 0.01 L at 165 K in ref 20 on thin films grown on Mo(001). This was interpreted as indirect evidence for water dissociation. Note, however, that the surface termination was not determined precisely in these studies. Turning back to Figure 3c, it is interesting that the intensity of the "reconstruction" spots maximizes simultaneously with the appearance of the (2 × 2) water ad-layer structure.

To shed light on the nature (thermodynamic vs kinetic) of the (2 × 2) structure observed during TP LEED measurements, we also looked at whether it may be obtained

DOI: 10.1021/acs.jpclett.9b00773
J. Phys. Chem. Lett. 2019, 10, 2487−2492

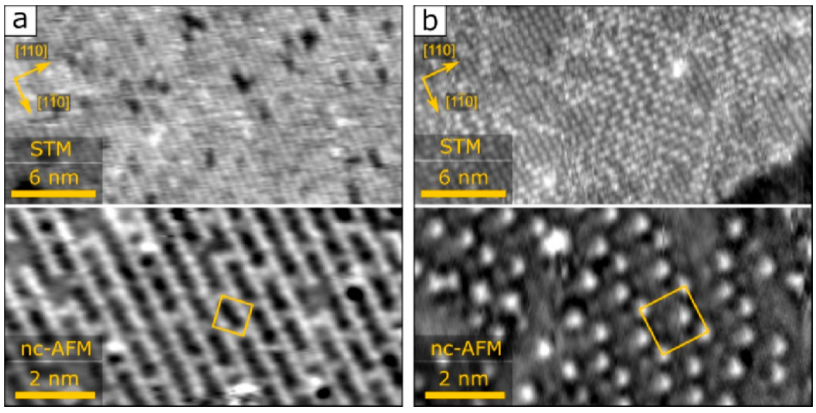

Figure 4. STM (top) and nc-AFM (bottom) images of high-coverage water structures on $Fe_3O_4(001)$ $(\sqrt{2} \times \sqrt{2})R45°$ surface. (a) At a coverage close to 6 H_2O/u.c., the protrusions on the surface exhibit the same $(\sqrt{2} \times \sqrt{2})R45°$ periodicity as the underlying surface. (b) When additional water is adsorbed (coverage 7−8 H_2O/u.c.), an array of bright protrusions with a (2×2) ordering emerges.

immediately upon water exposure. The results only showed faint (2×2) diffraction spots at low energies (25 eV) in a small range of water exposures between 1.5 and 2 L. According to the TPD results (Figure 3a), at this coverage the "monolayer" water film completes, and the formation of the ASW film sets in. However, the intensity of the (2×2) spots remarkably increases upon heating and subsequent desorption of ASW-related species. This finding suggests that (i) water ordering is promoted by surface diffusion and that (ii) the formation of the ASW film is not the prerequisite for the (2×2) ad-layer formation.

The formation of a (2×2) water ad-layer structure on the $Fe_3O_4(001)$-$(\sqrt{2} \times \sqrt{2})R45°$ surface observed here by LEED is further substantiated by scanning probe microscopy. Figure 4a shows scanning tunneling microscopy (STM) and non-contact atomic force microscopy (nc-AFM) images for a water coverage close to 6 H_2O per $(\sqrt{2} \times \sqrt{2})R45°$ unit cell (u.c.) (coverage calibration based on the previously reported quantitative TPD and DFT[17]). The STM image is dominated by rows running in the ⟨110⟩ directions, consistent with molecules being adsorbed at the surface Fe cations. nc-AFM using a CO-functionalized tip achieves superior resolution, and individual protrusions are discernible along the rows, along with additional protrusions located between the rows. The spacing of ∼11.8 Å is the repeat distance of the $(\sqrt{2} \times \sqrt{2})R45°$ unit cell in this direction, suggesting the water adlayer structure is defined by the surface reconstruction at this coverage. A DFT-based search[17] has previously shown that the most stable configuration at 6 H_2O/u.c. is a ring-like structure containing both molecular and dissociated water, with four species bound to the surface Fe cations, with a further two molecules stabilized at the bridge sites solely by hydrogen bonds. Figure 4b shows STM and AFM images when the coverage is increased slightly to 7−9 H_2O/u.c. Patches of the surface exhibit the (2×2) periodicity in STM and nc-AFM, as observed in LEED. Note that an additional protrusion is significantly offset from the center of the (2×2) cell. If it were in the center, this would correspond to $(\sqrt{2} \times \sqrt{2})R45°$ order. We infer that the new structure is not simply formed by the addition of water molecules to the existing 6 H_2O/u.c. structure and that additional reconfiguration must take place to optimize the hydrogen bonding network. Together with the TP LEED data, we conclude that the structure of the water adlayer is highly sensitive to the coverage.

STM and AFM studies of water adsorption on the (111) surface at low temperatures (to achieve high coverages corresponding to the ordered structure) are still missing. Such studies could verify the DFT-derived model of the water ad-layer, which is based on the cooperative formation of two-dimensional network of H-bonded dimers.[15] Nonetheless, in the light of the (2×2) structure formation, we mention previously reported STM images[21] obtained at room temperature on an $Fe_3O_4(111)$ single crystal exposed to ∼100 L at 110 K, which showed random short rows of water related protrusions separated by 12 Å, i.e., double the surface lattice constant. In addition, our own room-temperature STM images of $Fe_3O_4(111)$ films revealed water-related protrusions often showing a 12 Å periodicity (see Supporting Information). Therefore, it cannot be excluded that such structures, already formed in the initial stages of water adsorption, behave as the template for the long-range water ordering observed by LEED only at considerably higher coverages.

All in all, our results show that water forms ordered structures on both the $Fe_3O_4(111)$ and the $Fe_3O_4(001)$-$(\sqrt{2} \times \sqrt{2})R45°$ surfaces. Although ordered structures have been reported for a few water/oxide interfaces,[22−25] our study is the first to demonstrate the same phenomena on two major surfaces of the same oxide. While qualitative analysis of the LEED pattern allows us to identify structures with a surface symmetry different from the underlying oxide surface, we note that the intensity of the diffraction spots from the bare oxide surface (i.e., the (1×1) spots in Figure 2b and the R-spots in Figure 3c) remain almost the same at water coverage close to the onset of the ASW formation. This suggests that the final water adlayer most likely exhibits a "(1×1)" ordering at the highest coverages before multilayer growth sets in. Such structure have been predicted by DFT to be stable on the (111) surface.[15]

The (2×2) ad-layer structures observed on these two surfaces differ depending on the coverage and temperature at which they form. Apparently, the (2×2) structure on the $Fe_3O_4(001)$-$(\sqrt{2} \times \sqrt{2})R45°$ surface is less stable than on $Fe_3O_4(111)$ in terms of temperature window, i.e., 175−185 K versus 200−250 K, measured under the same experimental conditions. According to water coverage calibration done in ref 17, the $Fe_3O_4(001)$-(2×2) structure is observed at a coverage of about 8 H_2O/u.c., or 1.2×10^{15} H_2O/cm^2. For comparison, the $Fe_3O_4(111)$-(2×2) surface possesses about 1.75

DOI: 10.1021/acs.jpclett.9b00773
J. Phys. Chem. Lett. 2019, 10, 2487−2492

molecules per (1 × 1) unit cell, or 5.6 × 10^{14} H_2O/cm^2, i.e., about two times smaller.

Water adsorption on solids is usually rationalized in terms of competition between bonding to a (metal, oxide) surface and intermolecular H-bonding. Strong adsorption is often accompanied by water dissociation as in the case of $Fe_3O_4(111)$, for which both microcalorimetry and TPD results measured the adsorption energy about 100 kJ/mol.[16] Further adsorption occurs essentially on the hydroxyl precovered surface and results in half-dissociated dimers. According to the DFT calculations, H-bonding between water dimers further stabilizes the structure through the formation of a two-dimensional network, ultimately completing the first layer (monolayer). In top view, the network structure resembles the basal plane of hexagonal ice, observed on several (111)-oriented noble metal surfaces.[26−28] Note that on metal substrates the ice-like layer formation occurs from the onset as water adsorbs weakly, at least at low temperatures, so that H-bonding dominates in the formed structure.

According to the TPD results and also microcalorimetry data (to be published), initial water adsorption on the $Fe_3O_4(001)$-$(\sqrt{2} \times \sqrt{2})R45°$ surface is much weaker, about 70 kJ/mol, suggesting that water may adsorb molecularly at first. This would be consistent with the most recent DFT calculations,[17] which utilize the subsurface cation vacancy model for the surface structure. Isolated molecules were predicted to be slightly favored (by about 5 kJ/mol) over a dissociated molecule (E_{ads} = −57 kJ/mol). Moreover, the DFT analysis favors a partially dissociated water dimer (and trimer) when two (three) water molecules meet at the surface. Partial dissociation causes even stronger interaction with the metal cations such that the formation of a hexagonal ice layer on this surface seems unfavorable due to the square symmetry of the underlying oxide surface. Instead, a ring-like structure covering the surface follows the periodicity of the surface, suggesting water bonding to the metal dominates over H-bonding. According to the DFT-derived structures at the highest coverages, where (2 × 2) ordering is observed (see Figure 4), many water molecules coordinate without forming direct bonds to a substrate. It seems, therefore, that the observed ordered structure is metastable and intermediate between mono- and multilayer water films and forms when hydrogen bonds begin to dominate over the water−surface interaction.

In contrast, the formation of ice-like layer is rather natural on the $Fe_3O_4(111)$ surface having a proper surface symmetry. However, recent DFT calculations suggest that neither the symmetry of the OH patterns nor the similarity between a substrate and ice correlate well with the ice nucleation ability.[29] Instead, the OH density and the substrate−water interaction strength can be used as descriptors for ice to nucleate on a solid surface. Our results may shed some light on this issue.

EXPERIMENTAL SECTION

For studying reactivity of magnetite surfaces, we made use of well-ordered $Fe_3O_4(111)$[6,7,30] and $Fe_3O_4(001)$[12] thin films grown on Pt(111) and Pt(001), respectively. The experiments were performed in several ultrahigh vacuum (UHV) chambers (background pressures were below 2 × 10^{-10} mbar) in FHI (Berlin) and TU (Wien). In Berlin, the setup was equipped with standard facilities necessary to grow oxide films. TPD spectra were recorded using a quadrupole mass spectrometer (Hiden 301 3F) having a gold-plated cone shield in order to minimize signals from the heating stage. Water (D_2O, Sigma-Aldrich) was dosed using a directional doser. All samples were flashed in UHV to 900 K prior to water exposure.

The STM/nc-AFM experiments were performed on $Fe_3O_4(001)$ single crystals of natural origin (SurfaceNet GmbH). The samples were prepared by cycles of sputtering (1 keV Ar^+, 10 min) and annealing (900 K in UHV, with every other annealing step in a partial pressure of 1 × 10^{-6} mbar O_2 for 20 min). The STM image shown in Figure 4a and all nc-AFM images were acquired at 78 K using an Omicron LT STM equipped with a qPlus sensor. The STM image shown in Figure 4b was acquired in a different vacuum system using an Omicron LT STM with a standard STM setup. In both cases, sample preparation and water exposure were performed in a separate preparation chamber with a base pressure below 1 × 10^{-10} mbar. Water (H_2O) was exposed by backfilling the chamber using a high precision leak valve with the sample held at 150 K. Functionalization of the AFM tip with CO was performed in the manner described in ref 17.

ASSOCIATED CONTENT

Supporting Information

The Supporting Information is available free of charge on the ACS Publications website at DOI: 10.1021/acs.jpclett.9b00773.

STM images recorded at 300 K of water-contaminated $Fe_3O_4(111)$ surfaces (PDF)

AUTHOR INFORMATION

Corresponding Author

*E-mail: shaikhutdinov@fhi-berlin.mpg.de.

ORCID

Zdenek Jakub: 0000-0001-9538-9087
Francesca Mirabella: 0000-0001-8443-3652
Gareth S. Parkinson: 0000-0003-2457-8977
Shamil Shaikhutdinov: 0000-0001-9612-9949
Hans-Joachim Freund: 0000-0001-5188-852X

Notes

The authors declare no competing financial interest.

ACKNOWLEDGMENTS

This work has been supported by the Deutsche Forschungsgemeinschaft through SFB 1109 and by the Fonds der Chemischen Industrie. E.Z. thanks the International Max-Planck Research School "Functional Interfaces in Physics and Chemistry" for a fellowship. G.S.P. and Z.J. gratefully acknowledge funding from the Austrian Science Fund FWF (START-Prize Y 847-N20) and the Doctoral College TU-D (to Z.J.).

REFERENCES

(1) Henderson, M. A. The Interaction of Water With Solid Surfaces: Fundamental Aspects Revisited. *Surf. Sci. Rep.* **2002**, *46*, 1−308.
(2) Thiel, P. A.; Madey, T. E. The Interaction of Water With Solid Surfaces: Fundamental Aspects. *Surf. Sci. Rep.* **1987**, *7*, 211−385.
(3) Weiss, W.; Ranke, W. Surface Chemistry and Catalysis on Well-Defined Epitaxial Iron-Oxide Layers. *Prog. Surf. Sci.* **2002**, *70*, 1−151.
(4) Parkinson, G. S. Iron Oxide Surfaces. *Surf. Sci. Rep.* **2016**, *71*, 272−365.
(5) Kuhlenbeck, H.; Shaikhutdinov, S.; Freund, H.-J. Well-Ordered Transition Metal Oxide Layers in Model Catalysis − A Series of Case Studies. *Chem. Rev.* **2013**, *113*, 3986−4034.

DOI: 10.1021/acs.jpclett.9b00773
J. Phys. Chem. Lett. 2019, 10, 2487−2492

(6) Ritter, M.; Weiss, W. Fe_3O_4(111) Surface Structure Determined by LEED Crystallography. *Surf. Sci.* **1999**, *432*, 81−94.
(7) Shaikhutdinov, S. K.; Ritter, M.; Wang, X. G.; Over, H.; Weiss, W. Defect Structures on Epitaxial Fe_3O_4(111) films. *Phys. Rev. B: Condens. Matter Mater. Phys.* **1999**, *60*, 11062−11069.
(8) Sala, A.; Marchetto, H.; Qin, Z. H.; Shaikhutdinov, S.; Schmidt, T.; Freund, H. J. Defects and Inhomogeneities in Fe_3O_4(111) Thin Film Growth on Pt(111). *Phys. Rev. B: Condens. Matter Mater. Phys.* **2012**, *86*, 155430.
(9) Bliem, R.; McDermott, E.; Ferstl, P.; Setvin, M.; Gamba, O.; Pavelec, J.; Schneider, M. A.; Schmid, M.; Diebold, U.; Blaha, P.; Hammer, L.; Parkinson, G. S. Subsurface Cation Vacancy Stabilization of the Magnetite (001) Surface. *Science* **2014**, *346*, 1215−1218.
(10) Novotny, Z.; Mulakaluri, N.; Edes, Z.; Schmid, M.; Pentcheva, R.; Diebold, U.; Parkinson, G. Probing the Surface Phase Diagram of Fe_3O_4(001) Towards the Fe-rich Limit: Evidence for Progressive Reduction of the Surface. *Phys. Rev. B: Condens. Matter Mater. Phys.* **2013**, *87*, 195410.
(11) Pentcheva, R.; Moritz, W.; Rundgren, J.; Frank, S.; Schrupp, D.; Scheffler, M. A Combined DFT/LEED-Approach for Complex Oxide Surface Structure Determination: Fe_3O_4(001). *Surf. Sci.* **2008**, *602*, 1299−1305.
(12) Davis, E. M.; Zhang, K.; Cui, Y.; Kuhlenbeck, H.; Shaikhutdinov, S.; Freund, H.-J. Growth of Fe_3O_4(001) Thin Films on Pt(100): Tuning Surface Termination With an Fe Buffer Layer. *Surf. Sci.* **2015**, *636*, 42−46.
(13) Dementyev, P.; Dostert, K.-H.; Ivars-Barceló, F.; O'Brien, C. P.; Mirabella, F.; Schauermann, S.; Li, X.; Paier, J.; Sauer, J.; Freund, H.-J. Water Interaction with Iron Oxides. *Angew. Chem., Int. Ed.* **2015**, *54*, 13942−13946.
(14) Li, X.; Paier, J. Adsorption of Water on the Fe3O4(111) Surface: Structures, Stabilities, and Vibrational Properties Studied by Density Functional Theory. *J. Phys. Chem. C* **2016**, *120*, 1056−1065.
(15) Mirabella, F.; Zaki, E.; Ivars-Barcelo, F.; Li, X.; Paier, J.; Sauer, J.; Shaikhutdinov, S.; Freund, H.-J. Cooperative Formation of Long-Range Ordering in Water Ad-layers on Fe_3O_4(111). *Angew. Chem., Int. Ed.* **2018**, *57*, 1409−1413.
(16) Zaki, E.; Mirabella, F.; Ivars-Barceló, F.; Seifert, J.; Carey, S.; Shaikhutdinov, S.; Freund, H.-J.; Li, X.; Paier, J.; Sauer, J. Water Adsorption on the Fe_3O_4(111) surface: Dissociation and Network Formation. *Phys. Chem. Chem. Phys.* **2018**, *20*, 15764−15774.
(17) Meier, M.; Hulva, J.; Jakub, Z.; Pavelec, J.; Setvin, M.; Bliem, R.; Schmid, M.; Diebold, U.; Franchini, C.; Parkinson, G. S. Water Agglomerates on Fe_3O_4(001). *Proc. Natl. Acad. Sci. U. S. A.* **2018**, *115*, E5642−E5650.
(18) Parkinson, G. S.; Novotný, Z.; Jacobson, P.; Schmid, M.; Diebold, U. Room Temperature Water Splitting at the Surface of Magnetite. *J. Am. Chem. Soc.* **2011**, *133*, 12650−12655.
(19) Mulakaluri, N.; Pentcheva, R.; Wieland, M.; Moritz, W.; Scheffler, M. Partial Dissociation of Water on Fe_3O_4(001): Adsorbate Induced Charge and Orbital Order. *Phys. Rev. Lett.* **2009**, *103*, 176102.
(20) Liu, S.; Wang, S.; Li, W.; Guo, J.; Guo, Q. Water Dissociation on Magnetite (001) Films. *J. Phys. Chem. C* **2013**, *117*, 14070−14074.
(21) Cutting, R. S.; Muryn, C. A.; Vaughan, D. J.; Thornton, G. Substrate-termination and H_2O-coverage Dependent Dissociation of H_2O on Fe_3O_4(111). *Surf. Sci.* **2008**, *602*, 1155−1165.
(22) He, Y.; Tilocca, A.; Dulub, O.; Selloni, A.; Diebold, U. Local Ordering and Electronic Signatures of Submonolayer Water on Anatase TiO_2(101). *Nat. Mater.* **2009**, *8*, 585−589.
(23) Meyer, B.; Marx, D.; Dulub, O.; Diebold, U.; Kunat, M.; Langenberg, D.; Wöll, C. Partial Dissociation of Water Leads to Stable Superstructures on the Surface of Zinc Oxide. *Angew. Chem., Int. Ed.* **2004**, *43*, 6641−6645.
(24) Włodarczyk, R.; Sierka, M.; Kwapień, K.; Sauer, J.; Carrasco, E.; Aumer, A.; Gomes, J. F.; Sterrer, M.; Freund, H.-J. Structures of the Ordered Water Monolayer on MgO(001). *J. Phys. Chem. C* **2011**, *115*, 6764−6774.
(25) Zhao, X.; Shao, X.; Fujimori, Y.; Bhattacharya, S.; Ghiringhelli, L. M.; Freund, H.-J.; Sterrer, M.; Nilius, N.; Levchenko, S. V. Formation of Water Chains on CaO(001): What Drives the 1D Growth? *J. Phys. Chem. Lett.* **2015**, *6*, 1204−1208.
(26) Guo, J.; Bian, K.; Lin, Z.; Jiang, Y. Perspective: Structure and Dynamics of Water at Surfaces Probed by Scanning Tunneling Microscopy and Spectroscopy. *J. Chem. Phys.* **2016**, *145*, 160901.
(27) Tatarkhanov, M.; Ogletree, D. F.; Rose, F.; Mitsui, T.; Fomin, E.; Maier, S.; Rose, M.; Cerdá, J. I.; Salmeron, M. Metal- and Hydrogen-Bonding Competition During Water Adsorption on Pd(111) and Ru(0001). *J. Am. Chem. Soc.* **2009**, *131*, 18425−18434.
(28) Michaelides, A.; Morgenstern, K. Ice Nanoclusters at Hydrophobic Metal Surfaces. *Nat. Mater.* **2007**, *6*, 597.
(29) Pedevilla, P.; Fitzner, M.; Michaelides, A. What Makes a Good Descriptor for Heterogeneous Ice Nucleation on OH-patterned Surfaces. *Phys. Rev. B: Condens. Matter Mater. Phys.* **2017**, *96*, 115441.
(30) Weiss, W.; Ritter, M. Metal Oxide Heteroepitaxy: Stranski-Krastanov Growth for Iron Oxides on Pt(111). *Phys. Rev. B: Condens. Matter Mater. Phys.* **1999**, *59*, 5201−5213.

DOI: 10.1021/acs.jpclett.9b00773
J. Phys. Chem. Lett. 2019, 10, 2487−2492